PHOTONICS Research

Quantum nonreciprocality in quadratic optomechanics

Xunwei Xu,[1,*] Yanjun Zhao,[2] Hui Wang,[3] Hui Jing,[4,6] and Aixi Chen[1,5,7]

[1]Department of Applied Physics, East China Jiaotong University, Nanchang 330013, China
[2]Faculty of Information Technology, College of Microelectronics, Beijing University of Technology, Beijing 100124, China
[3]Center for Emergent Matter Science (CEMS), RIKEN, Wako, Saitama 351-0198, Japan
[4]Key Laboratory of Low-Dimensional Quantum Structures and Quantum Control of Ministry of Education, Department of Physics and Synergetic Innovation Center for Quantum Effects and Applications, Hunan Normal University, Changsha 410081, China
[5]Department of Physics, Zhejiang Sci-Tech University, Hangzhou 310018, China
[6]e-mail: jinghui73@foxmail.com
[7]e-mail: aixichen@zstu.edu.cn
*Corresponding author: davidxu0816@163.com

Received 2 July 2019; revised 28 October 2019; accepted 25 November 2019; posted 27 November 2019 (Doc. ID 371416); published 22 January 2020

We propose to achieve nonreciprocal quantum control of photons in a quadratic optomechanical (QOM) system based on directional nonlinear interactions. We show that by optically pumping the QOM system in one side, the effective QOM coupling can be enhanced significantly in that side, but not for the other side. This, contrary to the intuitive picture, allows the emergence of a nonreciprocal photon blockade in such optomechanical devices with weak single-photon QOM coupling. Our proposal opens up the prospect of exploring and utilizing quantum nonreciprocal optomechanics, with applications ranging from single-photon nonreciprocal devices to on-chip chiral quantum engineering.

https://doi.org/10.1364/PRJ.8.000143

1. INTRODUCTION

Optomechanical systems can be used to test the foundations of physics, and have important applications ranging from gravitational wave detections to quantum information processing (for reviews, see Refs. [1–6]). Recently, optomechanically induced nonreciprocity has been proposed theoretically [7–18] and demonstrated experimentally [19–28]. Nonreciprocal devices [29], such as isolators and circulators, have drawn an immense amount of interest in the past few years, for their irreplaceable role in signal processing and communication. An optomechanical system opens a route for nonreciprocity with nonlinear interactions [7,8,19,20], inherent non-trivial topology [9,21–24], and synthetic magnetism [10–18,25–28].

In this paper, we show that nonreciprocity can be realized in a whispering-gallery-mode (WGM) optomechanical system with quadratic optomechanical (QOM) coupling for quadratic mechanical-position dependent change in the optical frequency. Specifically, by optically pumping the quadratic WGM optomechanical system in one side, the effective QOM coupling can be enhanced significantly in that side, but not for the other side. The directional nonlinear interactions can induce nonreciprocal photon transport. This new possibility, as far as we know, has not been revealed in previous works.

It has been shown that the QOM systems driven by a strong optical driving field can generate strong (second-order) nonlinear photon-phonon interaction, even under weak single-photon optomechanical coupling conditions [30,31]. Nevertheless, we show here that the WGM optomechanical system with QOM coupling can be used to generate directional nonlinear interactions, which opens up the prospect of exploring nonreciprocal photon transport based on nonlinearity without the limitations of dynamic reciprocity [32]. Moreover, we demonstrate that directional nonlinear interactions can not only induce classical nonreciprocity, but also achieve nonreciprocal quantum control of photons by manipulating the statistic of the nonreciprocal transport photons.

Recently, a quantum nonreciprocal effect called nonreciprocal photon blockade (PB) was predicted theoretically [33] in a spinning Kerr resonator [34–37], that PB can emerge when the resonator is driven in one direction but not the other. Different from the nonreciprocal PB induced by the Fizeau–Sagnac drag [33], which relies on the condition of strong single-photon nonlinearity, here we show that the nonreciprocal PB can also be explored even with weak single-photon QOM coupling. Our proposal provides a feasible method to realize nonreciprocal photon blockade.

We note that the WGM optomechanical system has already been used for nonreciprocity with inherent non-trivial topology [9,21–24]. However, the WGM optomechanical systems with linear mechanical-position dependent change in the optical frequency (i.e., linear optomechanical coupling) can only enhance

linear photon-phonon interaction, which cannot be used to observe nonreciprocal PB. Our work provides not only a new platform (quadratic WGM optomechanics) but a new approach (i.e., directional nonlinear interaction) to designing nonreciprocal single-photon devices for backaction-immune quantum communication and chiral quantum photonics.

2. MODEL AND HAMILTONIAN

We note that the cavity frequency of a WGM optomechanical system is almost linearly proportional to the mechanical position [38,39], even though the effects of QOM coupling have also been observed in experiments [40,41]. The QOM coupling can facilitate nondestructive measurements of the energy of the mechanical oscillator [42,43], which is instead impossible for a system with linear optomechanical coupling. We present a scheme to generate QOM interactions in the normal optical modes of a WGM optomechanical system by eliminating the linear optomechanical couplings [44–47].

We consider a near-field cavity optomechanical setup consisting of one mechanical resonator optomechanically coupling to two optical resonators ($j = 1, 2$) via the optical evanescent field, with each optical resonator supporting two degenerate clockwise (CW) and counter-clockwise (CCW) travelling-wave WGMs, as shown in Figs. 1(a) and 1(b). The model can be described by the optomechanical interaction Hamiltonian

$$\begin{aligned} H_{\rm om} &= \sum_{j=1,2}\sum_{\lambda={\rm cw,\,ccw}} [\omega_0 + (-1)^j g_0 q] a^\dagger_{j,\lambda} a_{j,\lambda} \\ &\quad + J(a_{1,{\rm ccw}} a^\dagger_{2,{\rm cw}} + a_{1,{\rm cw}} a^\dagger_{2,{\rm ccw}} + {\rm H.c.}) \\ &\quad + \frac{1}{2}\omega_m (q^2 + p^2), \end{aligned} \tag{1}$$

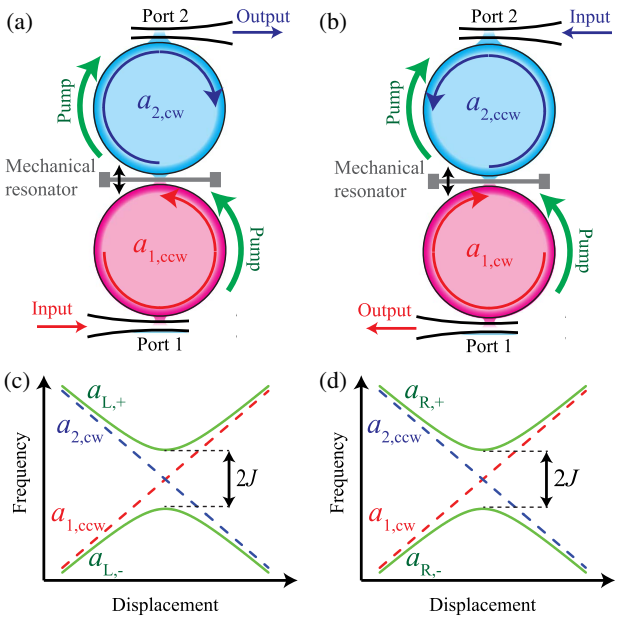

Fig. 1. (a), (b) Schematic diagram for generating QOM coupling, where a mechanical nanostring oscillator is placed between two whispering gallery mode (WGM) resonators. (c), (d) Dispersion of the optical modes as a function of the displacement.

where $a_{j,\lambda}$ and $a^\dagger_{j,\lambda}$ ($j = 1, 2$ and $\lambda = {\rm cw, ccw}$) are the annihilation and creation operators of the optical modes with frequency ω_0, and q and p are the dimensionless displacement and momentum operators of the mechanical resonator with frequency ω_m. As shown in Figs. 1(a) and 1(a), the mechanical resonator is placed at the middle of the gap of the two WGM resonators, so that the mechanical mode couples to the two WGM optical modes with linear optomechanical coupling of equal magnitude g_0 but opposite signs. Due to the tunneling coupling J between the optical modes, there is an avoided crossing for the optical resonance frequency, $\omega_\pm(q) = \omega_0 \pm \sqrt{J^2 + (g_0 q)^2}$, as shown in Figs. 1(c) and 1(d). We assume that the optical mode $a_{j,\lambda}$ is coupled to a waveguide (port j) with strength γ_c, and the damping rate of mechanical resonator q is γ_m. This theoretical model may also be realized with a membrane suspended on WGM microcavities [48] or photonic-crystal microcavities [49].

Following the approach in Refs. [44–47] (see Appendix A for more details), where $|J| \gg \omega_m$ is assumed such that q can be treated as a quasi-static variable, the Hamiltonian can be diagonalized quasi-statically as

$$\begin{aligned} H_{\rm om} &\approx (\omega_+ + g q^2)(a^\dagger_{L,+} a_{L,+} + a^\dagger_{R,+} a_{R,+}) \\ &\quad + (\omega_- - g q^2)(a^\dagger_{L,-} a_{L,-} + a^\dagger_{R,-} a_{R,-}) \\ &\quad + \frac{1}{2}\omega_m (q^2 + p^2) \end{aligned} \tag{2}$$

for normal modes $a_{R,\pm} \approx (a_{1,\rm cw} \pm a_{2,\rm ccw})/\sqrt{2}$ and $a_{L,\pm} \approx (a_{1,\rm ccw} \pm a_{2,\rm cw})/\sqrt{2}$ with eigenfrequencies $\omega_\pm(q) \approx \omega_0 \pm (J + g q^2)$ and single-photon QOM coupling $g \equiv g_0^2/(2J)$.

As already shown in the experiment [47], when the tunneling coupling between the optical modes is strong, i.e., $J > \gamma_c$, the transmission spectrum of a laser probe through the coupled optical modes features resonance dips at the normal resonance frequencies $\omega_\pm = \omega_0 \pm J$, not at the bare optical resonance frequencies ω_0. That is to say, the normal modes are coupled to the external waveguides and can be used to describe the input–output characteristic of the coupled optical modes system. Specifically, the normal modes $a_{L,\pm}$ and $a_{R,\pm}$ are coupled to both of the ports with strength $\gamma_c/2$, respectively, and the total damping rates are γ_c.

We can choose either pair of degenerated quasi-static normal optical modes ($a_{L,+}$ and $a_{R,+}$, or $a_{L,-}$ and $a_{R,-}$), to generate strong nonlinear interaction for a few photons travelling in one direction, but not in the reverse direction. Without loss of generality, the two optical modes are denoted as a_L and a_R, with frequency $\omega_a = \omega_+$ or ω_-, for photons travelling from port 1 to port 2 and the opposite direction, respectively. For example, to enhance the nonlinear optomechanical coupling between the optical mode a_L and the mechanical resonator b, the optical mode a_L is pumped by a strong field with amplitude Ω and frequency $\omega_L \sim \omega_a - 2\omega_m$. In the rotating reference frame with the optical frequency ω_L, the system can be described by

$$\begin{aligned} H_{\rm om+driv} &= (\Delta_a + g q^2)(a^\dagger_L a_L + a^\dagger_R a_R) + \frac{1}{2}\omega_m (q^2 + p^2) \\ &\quad + \Omega a^\dagger_L + \Omega a_L, \end{aligned} \tag{3}$$

with detuning $\Delta_a = \omega_a - \omega_L$. Under the strong driving condition $\Omega \gg \gamma_c$, we perform the displacement transformations: $a_L \to \alpha_L + a_L$, $a_R \to \alpha_R + a_R$, $q \to q_s + q$, and $p \to p_s + p$, where α_L, α_R, q_s, and p_s are the steady state values, and a_L, a_R, q, and p (on the right side of the arrow) are the quantum fluctuation operators. Adopting the standard linearization technique (see Appendix B), an effective Hamiltonian [30,31] for the quantum fluctuation operators is obtained as

$$H'_{\rm eff} = \Delta_a(a_L^\dagger a_L + a_R^\dagger a_R) + \omega'_m b^\dagger b + G a_L^\dagger b^2 + G^* a_L b^{\dagger 2}, \tag{4}$$

where $\omega'_m = \omega_m + g|\alpha_L|^2$ is the effective mechanical frequency, and $G = g\alpha_L/2$ is the effective (second-order) nonlinear coupling strength between the optical and mechanical modes. Without loss of generality, G is assumed to be real in the following.

To investigate the system's response behavior to a weak probe field, a weak field with amplitude $\varepsilon \ll \gamma_c$ and frequency $\omega_p \approx \omega_a$ is input from one of the ports. In the rotating reference frame with the unitary operator $R'(t) = \exp[i\delta(a_L^\dagger a_L + a_R^\dagger a_R + b^\dagger b/2)t]$, the total Hamiltonian is given by $H_{\rm tot} = H_{\rm eff} + H_{\rm probe}$, where

$$H_{\rm eff} = \Delta a_L^\dagger a_L + \Delta a_R^\dagger a_R + \Delta_m b^\dagger b + G a_L^\dagger b^2 + G^* a_L b^{\dagger 2}, \tag{5}$$

with detunings $\delta = \omega_p - \omega_L$, $\Delta = \Delta_a - \delta$, and $\Delta_m = \omega_m + g|\alpha_L|^2 - \delta/2$ satisfying the condition $\max\{|\Delta|, |\Delta_m|\} \ll \omega_m$. $H_{\rm probe} = \varepsilon a_\xi^\dagger + {\rm H.c.}$ describes the driving of the probe field with subscript $\xi = L$ for weak field input from port 1 and $\xi = R$ for weak field input from port 2. The effective Hamiltonian $H_{\rm eff}$ describes a directional nonlinear interaction between the optical and mechanical modes. If a probe field is input from port 1, the enhanced nonlinear interaction G between a_L and b may suppress the excitation of the second photon under a single-photon resonant condition. In contrast, by driving from port 2, as there is no strong nonlinear interaction between a_R and b, the photons are free to cross the system.

According to the input–output relations [50], we have $a_{1,\rm in} = \varepsilon/\sqrt{\gamma_c/2}$ and $a_{2,\rm out} = \sqrt{\gamma_c/2}a_L$ ($a_{2,\rm in} = \varepsilon/\sqrt{\gamma_c/2}$ and $a_{1,\rm out} = \sqrt{\gamma_c/2}a_R$), and then the transmission coefficient for the weak probe field can be defined by

$$T_{21} \equiv \frac{\langle a_{2,\rm out}^\dagger a_{2,\rm out}\rangle}{\langle a_{1,\rm in}^\dagger a_{1,\rm in}\rangle} = \frac{\gamma_c^2}{4\varepsilon^2}\langle a_L^\dagger a_L\rangle, \tag{6}$$

for photon transport from port 1 to port 2, and

$$T_{12} \equiv \frac{\langle a_{1,\rm out}^\dagger a_{1,\rm out}\rangle}{\langle a_{2,\rm in}^\dagger a_{2,\rm in}\rangle} = \frac{\gamma_c^2}{4\varepsilon^2}\langle a_R^\dagger a_R\rangle, \tag{7}$$

for photon transport from port 2 to port 1, where $n_L \equiv \langle a_L^\dagger a_L\rangle$ and $n_R \equiv \langle a_R^\dagger a_R\rangle$ are the mean photon numbers. The isolation for probe field transport from port 1 to port 2 is defined by $I \equiv T_{21}/T_{12}$. Using the input–output relations, the statistic properties of the transmitted photons $a_{2,\rm out}$ and $a_{1,\rm out}$ can be described by the second-order correlation functions in the steady state ($t \to \infty$) as follows:

$$g_{21}^{(2)}(\tau) \equiv \frac{\langle a_{2,\rm out}^\dagger(t) a_{2,\rm out}^\dagger(t+\tau) a_{2,\rm out}(t+\tau) a_{2,\rm out}(t)\rangle}{\langle a_{2,\rm out}^\dagger(t) a_{2,\rm out}(t)\rangle^2} = \frac{\langle a_L^\dagger(t) a_L^\dagger(t+\tau) a_L(t+\tau) a_L(t)\rangle}{\langle a_L^\dagger(t) a_L(t)\rangle^2}, \tag{8}$$

for photon transport from port 1 to port 2, and

$$g_{12}^{(2)}(\tau) \equiv \frac{\langle a_{1,\rm out}^\dagger(t) a_{1,\rm out}^\dagger(t+\tau) a_{1,\rm out}(t+\tau) a_{1,\rm out}(t)\rangle}{\langle a_{1,\rm out}^\dagger(t) a_{1,\rm out}(t)\rangle^2} = \frac{\langle a_R^\dagger(t) a_R^\dagger(t+\tau) a_R(t+\tau) a_R(t)\rangle}{\langle a_R^\dagger(t) a_R(t)\rangle^2}, \tag{9}$$

for photon transport from port 2 to port 1.

3. NONRECIPROCAL PB

The transmission coefficients and correlation functions can be obtained by numerically solving the master equation for the density matrix ρ of the system [51]

$$\frac{\partial \rho}{\partial t} = -i[H_{\rm tot}, \rho] + \gamma_c L[a_L]\rho + \gamma_c L[a_R]\rho + \gamma_m(n_{\rm th}+1)L[b]\rho + \gamma_m n_{\rm th} L[b^\dagger]\rho, \tag{10}$$

where $L[o]\rho = o\rho o^\dagger - (o^\dagger o\rho + \rho o^\dagger o)/2$ denotes a Lindbland term for an operator o, and $n_{\rm th}$ is the mean thermal phonon number, given by the Bose–Einstein statistics $n_{\rm th} = [\exp(\hbar\omega_m/k_B T) - 1]^{-1}$ with the Boltzmann constant k_B and the temperature T of the reservoir at the thermal equilibrium.

In Fig. 2(a), we show the transmission coefficients T_{21} for probe field transport from port 1 to port 2, and T_{12} for probe field transport from port 2 to port 1 versus the detuning Δ/G. For T_{21}, there are two peaks at $\Delta = \pm\sqrt{2}G$ and one dip at

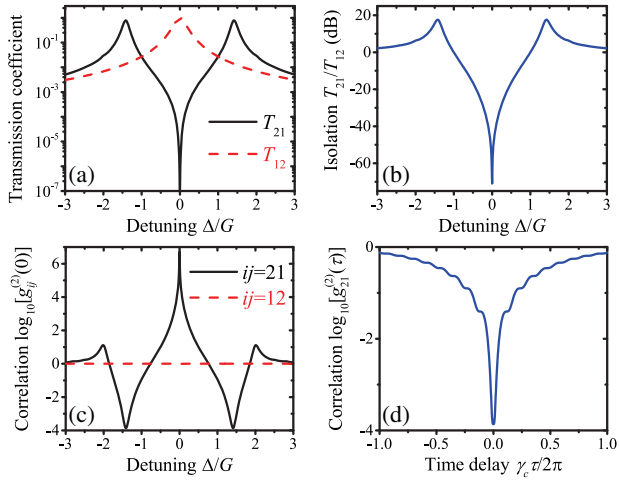

Fig. 2. (a) The transmission coefficients T_{21} (solid black curve) and T_{12} (dashed red curve) as a function of the detuning Δ/G. (b) The isolation as a function of the detuning Δ/G. (c) The equal-time second-order correlation function $\log_{10}[g_{ij}^{(2)}(0)]$ ($ij = 12, 21$) as a function of the detuning Δ/G. (d) The second-order correlation function $\log_{10}[g_{21}^{(2)}(\tau)]$ as a function of the normalized time delay $\gamma_c\tau/(2\pi)$ at detuning $\Delta = \sqrt{2}G$. The other parameters are $\Delta_m = \Delta/2$, $G = 3\gamma_c$, $\varepsilon = \gamma_c/10$, $\gamma_m = \gamma_c/100$, and $n_{\rm th} = 0$.

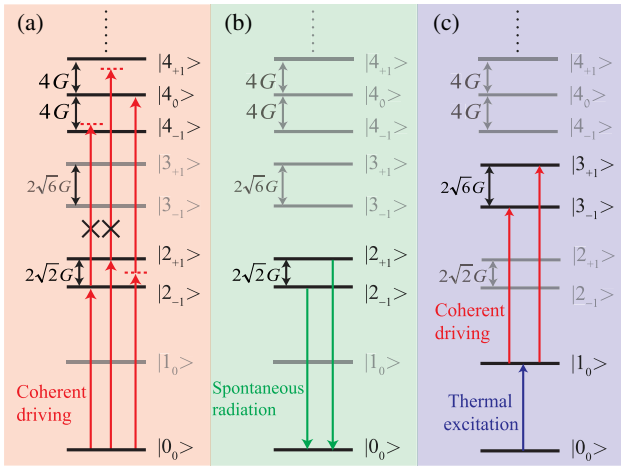

Fig. 3. Schematic energy spectrum of the linearized QOM coupling between optical mode a_L and mechanical resonator b, where $|0_0\rangle \equiv |0,0\rangle$, $|1_0\rangle \equiv |0,1\rangle$, $|2_{\pm1}\rangle \equiv (|1,0\rangle \pm |0,2\rangle)/\sqrt{2}$, $|3_{\pm1}\rangle \equiv (|1,1\rangle \pm |0,3\rangle)/\sqrt{2}$, $|4_0\rangle \equiv (-\sqrt{3}|2,0\rangle + |0,4\rangle)/2$, $|4_{\pm1}\rangle \equiv (|2,0\rangle \pm 2|1,2\rangle + \sqrt{3}|0,4\rangle)/(2\sqrt{2})$, and $|n,m\rangle$ represents the Fock state with n photons in a_L and m phonons in b.

$\Delta = 0$. In contrast, there is only one peak at $\Delta = 0$ for T_{12}. Figure 2(b) shows the isolation $I = T_{21}/T_{12}$ for probe field transport from port 1 to port 2 as a function of the detuning Δ/G. The isolation for the direction $1 \to 2$ is more than 17 dB at detuning $\Delta = \pm\sqrt{2}G$, and the isolation for the reverse direction $2 \to 1$, i.e., $\tilde{I} \equiv T_{12}/T_{21}$, is more than 70 dB at detuning $\Delta = 0$.

To explore the statistic properties of the transmitted photons, the equal-time second-order correlation function $\log_{10}[g_{ij}^{(2)}(0)]$ $(ij = 12, 21)$ is shown as a function of the detuning Δ/G in Fig. 2(c). The photon transport from port 2 to port 1 is coherent in full frequency, i.e., $g_{12}^{(2)}(0) = 1$. The photon transport from port 1 to port 2 exhibits strong antibunching effect, i.e., $g_{21}^{(2)}(0) \ll 1$, around the detunings $\Delta = \pm\sqrt{2}G$, and exhibits strong bunching effect, i.e., $g_{21}^{(2)}(0) \gg 1$, around the detunings $\Delta = 0$ and $\pm 2G$. The time duration for nonreciprocal PB at $\Delta = \pm\sqrt{2}G$ is on the order of $2\pi/(10\gamma_c)$, as shown in Fig. 2(d).

The peak for $T_{12} \approx 1$ at detuning $\Delta = 0$ can be understood by the fact that when the probe field is injected from port 2, only the (linear) optical mode a_R can be excited. Thus the maximum transmission coefficient is reached for the probe field in resonance with the optical mode a_R, i.e., $\Delta = 0$, and the transmitted photons keep the statistic properties of the probe field (a coherent field), i.e., $g_{12}^{(2)}(0) = 1$, as there is no nonlinear interaction in the optical path from port 2 to port 1.

In order to understand the origin of the peak for $T_{21} \approx 0.8$ around the detuning $\Delta = \pm\sqrt{2}G$ and the dip for $T_{21} \approx 10^{-7}$ at $\Delta = 0$, we show energy spectrum (see Appendix C) of the linearized QOM coupling between optical mode a_L and mechanical resonator b in Fig. 3. Under weak probe condition, the maximum transmission coefficient $T_{21} \approx 0.8$ is reached for the probe field in resonance with the transition $|0_0\rangle \to |2_{\pm1}\rangle$, i.e., $\Delta = \pm\sqrt{2}G$, as shown in Fig. 3(a). However, the photon absorbed in the transition $|0_0\rangle \to |2_{\pm1}\rangle$ blocks the transition $|2_{\pm1}\rangle \to |4_{\pm1}\rangle$ for large detuning, so we have $g_{12}^{(2)}(0) \ll 1$ around the detuning $\Delta = \pm\sqrt{2}G$. The dip for $T_{21} \approx 10^{-7}$ at $\Delta = 0$ arises from the quantum interference between the transitions $|2_{+1}\rangle \to |0_0\rangle$ and $|2_{-1}\rangle \to |0_0\rangle$ [Fig. 3(b)], in an equivalent picture as optomechanically induced transparency [52–54], or electromagnetically induced transparency in lambda-type three-level atoms [55,56]. Moreover, when $\Delta = 0$, the transition $|0_0\rangle \to |2_{\pm1}\rangle$ is suppressed, but the two-photon transition $|0_0\rangle \to |4_0\rangle$ is resonant, which induces two-photon tunneling from port 1 to point 2, i.e., $g_{21}^{(2)}(0) \gg 1$. Similarly, $g_{21}^{(2)}(0) \gg 1$ around $\Delta = \pm 2G$ is induced by the resonant transition $|0_0\rangle \to |4_\pm\rangle$.

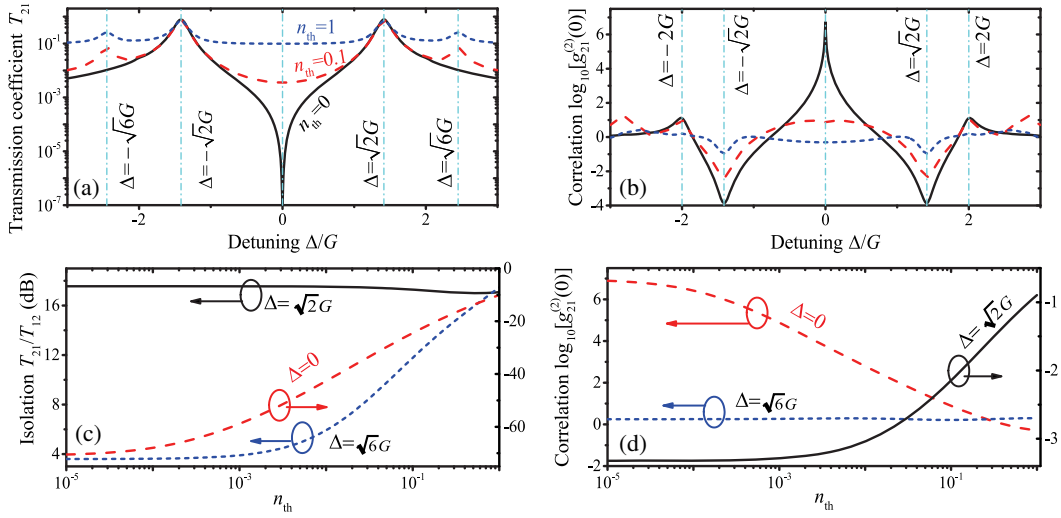

Fig. 4. (a) Transmission coefficient T_{21}. (b) The equal-time second-order correlation function $\log_{10}[g_{21}^{(2)}(0)]$ versus the detuning Δ/G with different mean thermal phonon number $(n_{th} = 0, 0.1, 1)$. (c) The isolation T_{21}/T_{12}. (d) The equal-time second-order correlation function $\log_{10}[g_{21}^{(2)}(0)]$ versus the mean thermal phonon number n_{th} with different detuning $(\Delta = 0, \sqrt{2}G, \sqrt{6}G)$. The other parameters are the same as in Fig. 2.

We now discuss the effect of thermal phonons on the nonreciprocal PB. Figures 4(a) and 4(b) show the transmission coefficient T_{21} and the equal-time second-order correlation function $\log_{10}[g_{21}^{(2)}(0)]$ versus the detuning Δ/G with a different mean thermal phonon number ($n_{\rm th}=0,0.1,1$). Thermal phonons have little influence on the transmission coefficient T_{21} around $\Delta=\pm\sqrt{2}G$, but have great effect on the transmission coefficient T_{21} around $\Delta=0$. Thermal phonons have great effect on the second-order correlation function $\log_{10}[g_{21}^{(2)}(0)]$ around $\Delta=0$ and $\pm\sqrt{2}G$.

The isolation T_{21}/T_{12} and the second-order correlation function $\log_{10}[g_{21}^{(2)}(0)]$ versus the mean thermal phonon number $n_{\rm th}$ are shown in Figs. 4(c) and 4(d) with detuning $\Delta=0$, $\sqrt{2}G,\sqrt{6}G$. The isolation T_{21}/T_{12} around $\Delta=\sqrt{2}G$ is robust against the thermal phonons, but the antibunching effect of the transport photons becomes much weaker for greater thermal phonons. Both the isolation T_{21}/T_{12} and second-order correlation function $\log_{10}[g_{21}^{(2)}(0)]$ around $\Delta=0$ are sensitive to the mean thermal phonon number $n_{\rm th}$, and this quality may be used in accurate temperature measurement at ultra-low temperature.

More interestingly, two peaks appear around $\Delta=\pm\sqrt{6}G$ in the transmission coefficient T_{21}, and the isolation T_{21}/T_{12} can be improved with a larger thermal phonon number $n_{\rm th}$. This abnormal effect is induced by the phonon states, e.g., $|1_0\rangle$ in Fig. 3(c). As the temperature increases, the population probability in phonon state $|1_0\rangle$ increases, and the transitions of $|1_0\rangle\rightarrow|3_{\pm1}\rangle$ with resonance frequency $\Delta=\pm\sqrt{6}G$ become remarkable gradually, which induces the increasing peaks of the transmission coefficient T_{21} (or the isolation T_{21}/T_{12}) around $\Delta=\pm\sqrt{6}G$.

4. DISCUSSIONS AND CONCLUSIONS

Let us now discuss the experimental requirements for our proposal. Considering the parameters from a recent near-field WGM optomechanical experiment [39]: $g_0\sim 2\pi\times(10\text{–}100)$ kHz, $\gamma_c\sim 2\pi\times(100\text{–}1000)$ MHz, and $J\approx 2\pi\times 1000$ MHz for strong coupling, we have QOM coupling $g/2\pi\sim 10$ Hz, which is too weak to realize $G=g\alpha_L/2>\gamma_c$. However, many schemes have been proposed to enhance the optomechanical coupling g_0 in recent years, such as by using the collective mechanical modes in scatter arrays [57], the squeezed cavity mode [58], or the Josephson effect for electromechanical systems [59]. The optomechanical coupling g_0 can be enhanced by several orders of magnitude and the strong coupling regime ($g_0>\gamma_c$) can even be approached [57–59]. Furthermore, the frequency range of the SiN nanostring oscillators in the near-field cavity optomechanical setup is about 0.1–10 MHz [38–41], which is too low to observe nonreciprocal PB. One possible solution is replaying the SiN nanostring oscillator with an optomechanical crystal nanobeam, as optomechanical crystal nanobeams with GHz mechanical modes have been designed and demonstrated recently [60,61]. Moreover, the thermal phonons have important influence on the nonreciprocal PB, and the thermal effect can be suppressed for higher frequency mechanical mode.

In addition, there are two driving fields coupling to the system with frequencies $\omega_L\sim\omega_a-2\omega_m$ and $\omega_p\sim\omega_a$, and the strengths $\Omega\gg\varepsilon$. In order to detect the photon correlation induced by the weak probe field, we should spectrally filter out the strong optical driving field at frequency ω_L under the condition $\omega_a-\omega_L\gg\{\gamma_c,G\}$. A similar method has already been used to measure correlations of phonons in a recent experiment [62].

In summary, we have shown that the WGM optomechanical system with QOM coupling can be used to obtain directional nonlinear interactions and observe nonreciprocal PB. In addition, the thermal phonons have important influence on the nonreciprocal PB, especially on the statistic properties of the transport photons, and this quality may be used in temperature sensing at ultra-low temperature. Moreover, this work can be extended to study phonon manipulation in double-cavity optomechanics, e.g., nonreciprocal phonon blockades [63], nonreciprocal phonon lasers [64–70], nonreciprocal photon-phonon entanglements and quantum transfers. Directional nonlinear interaction can also be applied in the high-Q microtoroid resonator with phase-matched parametric amplification [71] or superconducting microwave circuit with Josephson parametric converters [72] to achieve nonreciprocal quantum control of photons. Our proposal provides a new routine towards the realization of on-chip quantum nonreciprocal devices, backaction-immune quantum measurement, and chiral quantum physics.

APPENDIX A: QUADRATIC OPTOMECHANICAL COUPLING

To realize quantum nonreciprocality in optomechanics, we consider a near-field cavity optomechanical setup consisting of one mechanical resonator optomechanical coupling to two optical resonators ($j=1,2$) via the optical evanescent field, with each optical resonator supporting two degenerate clockwise (CW) and counter-clockwise (CCW) travelling-wave whispering-galley-modes (WGMs). The model can be described by the optomechanical interaction Hamiltonian

$$\begin{aligned}H_{\rm om}=&\begin{pmatrix}a_{1,\rm ccw}^{\dagger} & a_{2,\rm cw}^{\dagger}\end{pmatrix}\begin{pmatrix}\omega_0-g_0q & J\\ J & \omega_0+g_0q\end{pmatrix}\begin{pmatrix}a_{1,\rm ccw}\\ a_{2,\rm cw}\end{pmatrix}\\&+\begin{pmatrix}a_{1,\rm cw}^{\dagger} & a_{2,\rm ccw}^{\dagger}\end{pmatrix}\begin{pmatrix}\omega_0-g_0q & J\\ J & \omega_0+g_0q\end{pmatrix}\begin{pmatrix}a_{1,\rm cw}\\ a_{2,\rm ccw}\end{pmatrix}\\&+\frac{1}{2}\omega_m(q^2+p^2),\end{aligned}\tag{A1}$$

where $a_{j,\lambda}$ and $a_{j,\lambda}^{\dagger}$ ($j=1,2$ and $\lambda=\rm cw,ccw$) are the annihilation and creation operators of the optical modes with frequency ω_0, J is the tunneling amplitude between the optical modes, q and p are the dimensionless displacement and momentum operators of the mechanical resonator with frequency ω_m, and g_0 is the linear optomechanical coupling strength between the mechanical resonator and optical modes. We assume that the optical mode $a_{j,\lambda}$ is coupled to a waveguide (port j) with strength γ_c, and the damping rate of mechanical resonator q is γ_m.

The Hamiltonian in Eq. (A1) can be diagonalized as

$$H_{\rm om} = \begin{pmatrix} a_{L,+}^{\dagger} & a_{L,-}^{\dagger} \end{pmatrix} \begin{pmatrix} \omega_+(q) & 0 \\ 0 & \omega_-(q) \end{pmatrix} \begin{pmatrix} a_{L,+} \\ a_{L,-} \end{pmatrix} + \begin{pmatrix} a_{R,+}^{\dagger} & a_{R,-}^{\dagger} \end{pmatrix} \begin{pmatrix} \omega_+(q) & 0 \\ 0 & \omega_-(q) \end{pmatrix} \begin{pmatrix} a_{R,+} \\ a_{R,-} \end{pmatrix} + \frac{1}{2}\omega_m(q^2+p^2), \tag{A2}$$

in the normal modes basis,

$$a_{L,\pm} = \frac{1}{D_\pm}\left[J a_{1,\rm ccw} + \left(g_0 q \pm \sqrt{J^2+(g_0 q)^2}\right) a_{2,\rm cw}\right] \tag{A3}$$

and

$$a_{R,\pm} = \frac{1}{D_\pm}\left[J a_{1,\rm cw} + \left(g_0 q \pm \sqrt{J^2+(g_0 q)^2}\right) a_{2,\rm ccw}\right], \tag{A4}$$

with

$$D_\pm^2 = J^2 + \left(g_0 q \pm \sqrt{J^2+(g_0 q)^2}\right)^2, \tag{A5}$$

and eigenfrequencies

$$\omega_\pm(q) = \omega_0 \pm \sqrt{J^2+(g_0 q)^2}. \tag{A6}$$

Moreover, $|J| \gg g_0 q$ is assumed [44–47] such that we can Taylor-expand the eigenfrequencies in Eq. (A6) as

$$\omega_\pm(q) \approx \omega_\pm \pm \frac{g_0^2}{2J} q^2, \tag{A7}$$

with frequencies $\omega_\pm \equiv \omega_\pm(0) = \omega_0 \pm J$, and the quasi-static Hamiltonian in Eq. (A2) is given approximately by Eq. (2) in the main text with quadratic optomechanical coupling $g \equiv g_0^2/(2J)$, and quasi-static normal optical modes, $a_{L,\pm} \approx (a_{1,\rm ccw} \pm a_{2,\rm cw})/\sqrt{2}$ and $a_{R,\pm} \approx (a_{1,\rm cw} \pm a_{2,\rm ccw})/\sqrt{2}$.

APPENDIX B: LINEARIZED OPTOMECHANICAL HAMILTONIAN

We consider a pair of degenerated quasi-static normal optical modes ($a_{L,+}$ and $a_{R,+}$, or $a_{L,-}$ and $a_{R,-}$), to generate strong nonlinear interaction for a few photons travelling in one direction, but not in the reverse direction. Without loss of generality, the two optical modes are denoted as a_L and a_R, with frequency $\omega_a = \omega_+$ or ω_-, for photons travelling from port 1 to port 2 and the opposite direction, respectively. For example, to enhance the nonlinear optomechanical coupling between the optical mode a_L and the mechanical resonator, the optical mode a_L is pumped by a strong field with amplitude Ω and frequency $\omega_L \sim \omega_a - 2\omega_m$. In the rotating reference frame with the optical frequency ω_L, the system can be described by Eq. (3) in the main text with detuning $\Delta_a = \omega_a - \omega_L$.

Under strong driving condition $\Omega \gg \gamma_c$, we perform the displacement transformations: $a_L \to \alpha_L + a_L$, $a_R \to \alpha_R + a_R$, $q \to q_s + q$, and $p \to p_s + p$, where α_L, α_R, q_s, and p_s are the steady state values, and a_L, a_R, q, and p (on the right side of the arrow) are the quantum fluctuation operators. The steady state values α_L, α_R, q_s, and p_s can be obtained by the equations of motions yielding

$$\alpha_L = \frac{-i2\Omega}{\gamma_c + i2\Delta_a} \tag{B1}$$

and

$$\alpha_R = q_s = p_s = 0. \tag{B2}$$

The operators q and p for the mechanical resonator can be written in terms of phonon creation and annihilation operators as $q = (b^\dagger + b)/\sqrt{2}$, $p = i(b^\dagger - b)/\sqrt{2}$, and the effective Hamiltonian for the quantum fluctuation operators reads

$$H'_{\rm eff} = \Delta_a a_L^\dagger a_L + \Delta_a a_R^\dagger a_R + \omega_m b^\dagger b + \frac{g}{2}(|\alpha_L|^2 + a_L^\dagger a_L + a_R^\dagger a_R)(b^\dagger + b)^2 + \frac{g}{2}(\alpha_L a_L^\dagger + \alpha_L^* a_L)(b^\dagger + b)^2. \tag{B3}$$

We assume that the optical driving field is strong enough so we have $|\alpha_L|^2 \gg \langle a_L^\dagger a_L\rangle \sim \langle a_R^\dagger a_R\rangle$, and so that the term $g(a_L^\dagger a_L + a_R^\dagger a_R)(b^\dagger + b)^2$ in the above equation can be neglected safely. For $\Delta_a \sim 2\omega_m \gg |g\alpha_L|/2$, the effective Hamiltonian can be further simplified by rotating-wave approximation and neglecting the high frequency terms [30,31], e.g., b^2 and ab^2. Then, we get Eq. (4) in the main text, where $\omega_m' = \omega_m + g|\alpha_L|^2$ is the effective mechanical frequency, and $G = g\alpha_L/2$ is the effective nonlinear coupling strength between the optical and mechanical modes.

APPENDIX C: ENERGY SPECTRUM

In this appendix, we will show the energy spectrum of the effective Hamiltonian in the diagonal basis under the condition $\Delta = 2\Delta_m$, and similar results are shown in Refs. [30,31]. In the noncoupling basis, $|n, m\rangle$ represents the Fock state with n photons in a_L and m phonons in b. It is clear that the vacuum state

$$|0_0\rangle \equiv |0, 0\rangle \tag{C1}$$

and the single-phonon state

$$|1_0\rangle \equiv |0, 1\rangle, \tag{C2}$$

are decoupled from the other states. The degenerate states $|1, 0\rangle$ and $|0, 2\rangle$ are coupled with strengh $\sqrt{2}G$, so the eigenstates are

$$|2_{\pm 1}\rangle \equiv \frac{1}{\sqrt{2}}(|1, 0\rangle \pm |0, 2\rangle), \tag{C3}$$

with energy splitting

$$\Delta_{2,\pm} = \pm\sqrt{2}G. \tag{C4}$$

The degenerate states $|1, 1\rangle$ and $|0, 3\rangle$ are coupled with strength $\sqrt{6}G$, so the eigenstates are

$$|3_{\pm 1}\rangle \equiv \frac{1}{\sqrt{2}}(|1, 1\rangle \pm |0, 3\rangle), \tag{C5}$$

with energy splitting

$$\Delta_{3,\pm} = \pm\sqrt{6}G. \tag{C6}$$

The states $|2, 0\rangle$, $|1, 2\rangle$, and $|0, 4\rangle$ are degenerate, where $|2, 0\rangle$ and $|1, 2\rangle$ are coupled with strength $2G$, and $|0, 4\rangle$

and $|1,2\rangle$ are coupled with strength $2\sqrt{3}G$, so the eigenstates are

$$|4_0\rangle \equiv \frac{1}{2}\left(-\sqrt{3}|2,0\rangle + |0,4\rangle\right), \tag{C7}$$

$$|4_{\pm 1}\rangle \equiv \frac{1}{2\sqrt{2}}\left(|2,0\rangle \pm 2|1,2\rangle + \sqrt{3}|0,4\rangle\right), \tag{C8}$$

with energy splitting

$$\Delta_{4,0} = 0, \tag{C9}$$

$$\Delta_{4,\pm} = \pm 4G. \tag{C10}$$

The schematic energy spectrum in the diagonal basis is given in Fig. 3.

Funding. Natural Science Foundation of Jiangxi Province (20192ACB21002); National Natural Science Foundation of China (11604096, 11904013, 11847165, 11474087, 11774086, 11935006, 11775190).

REFERENCES

1. T. J. Kippenberg and K. J. Vahala, "Cavity optomechanics: back-action at the mesoscale," Science **321**, 1172–1176 (2008).
2. F. Marquardt and S. M. Girvin, "Optomechanics," Physics **2**, 40 (2009).
3. M. Aspelmeyer, P. Meystre, and K. Schwab, "Quantum optomechanics," Phys. Today **65**, 29–35 (2012).
4. M. Aspelmeyer, T. J. Kippenberg, and F. Marquardt, "Cavity optomechanics," Rev. Mod. Phys. **86**, 1391–1452 (2014).
5. M. Metcalfe, "Applications of cavity optomechanics," Appl. Phys. Rev. **1**, 031105 (2014).
6. Y.-L. Liu, C. Wang, J. Zhang, and Y.-X. Liu, "Cavity optomechanics: manipulating photons and phonons towards the single-photon strong coupling," Chin. Phys. B **27**, 024204 (2018).
7. S. Manipatruni, J. T. Robinson, and M. Lipson, "Optical nonreciprocity in optomechanical structures," Phys. Rev. Lett. **102**, 213903 (2009).
8. H. Qiu, J. Dong, L. Liu, and X. Zhang, "Energy-efficient on-chip optical diode based on the optomechanical effect," Opt. Express **25**, 8975–8985 (2017).
9. M. Hafezi and P. Rabl, "Optomechanically induced non-reciprocity in microring resonators," Opt. Express **20**, 7672–7684 (2012).
10. M. Schmidt, S. Kessler, V. Peano, O. Painter, and F. Marquardt, "Optomechanical creation of magnetic fields for photons on a lattice," Optica **2**, 635–641 (2015).
11. A. Metelmann and A. A. Clerk, "Nonreciprocal photon transmission and amplification via reservoir engineering," Phys. Rev. X **5**, 021025 (2015).
12. X.-W. Xu and Y. Li, "Optical nonreciprocity and optomechanical circulator in three-mode optomechanical systems," Phys. Rev. A **91**, 053854 (2015).
13. K. Fang, M. Matheny, X. Luan, and O. Painter, "Optical transduction and routing of microwave phonons in cavity-optomechanical circuits," Nat. Photonics **10**, 489–496 (2016).
14. X.-W. Xu, Y. Li, A.-X. Chen, and Y.-X. Liu, "Nonreciprocal conversion between microwave and optical photons in electro-optomechanical systems," Phys. Rev. A **93**, 023827 (2016).
15. A. Metelmann and A. A. Clerk, "Nonreciprocal quantum interactions and devices via autonomous feedforward," Phys. Rev. A **95**, 013837 (2017).
16. L. Tian and Z. Li, "Nonreciprocal quantum-state conversion between microwave and optical photons," Phys. Rev. A **96**, 013808 (2017).
17. M.-A. Miri, F. Ruesink, E. Verhagen, and A. Alù, "Optical nonreciprocity based on optomechanical coupling," Phys. Rev. Appl. **7**, 064014 (2017).
18. G. Li, X. Xiao, Y. Li, and X. Wang, "Tunable optical nonreciprocity and a phonon-photon router in an optomechanical system with coupled mechanical and optical modes," Phys. Rev. A **97**, 023801 (2018).
19. J. Kim, M. C. Kuzyk, K. Han, H. Wang, and G. Bahl, "Non-reciprocal Brillouin scattering induced transparency," Nat. Phys. **11**, 275–280 (2015).
20. C.-H. Dong, Z. Shen, C.-L. Zou, Y.-L. Zhang, W. Fu, and G.-C. Guo, "Brillouin-scattering-induced transparency and non-reciprocal light storage," Nat. Commun. **6**, 6193 (2015).
21. Z. Shen, Y.-L. Zhang, Y. Chen, C.-L. Zou, Y.-F. Xiao, X.-B. Zou, F.-W. Sun, G.-C. Guo, and C.-H. Dong, "Experimental realization of optomechanically induced non-reciprocity," Nat. Photonics **10**, 657–661 (2016).
22. F. Ruesink, M.-A. Miri, A. Alù, and E. Verhagen, "Nonreciprocity and magnetic-free isolation based on optomechanical interactions," Nat. Commun. **7**, 13662 (2016).
23. Z. Shen, Y.-L. Zhang, Y. Chen, F.-W. Sun, X.-B. Zou, G.-C. Guo, C.-L. Zou, and C.-H. Dong, "Reconfigurable optomechanical circulator and directional amplifier," Nat. Commun. **9**, 1797 (2018).
24. F. Ruesink, J. P. Mathew, M.-A. Miri, A. Alù, and E. Verhagen, "Optical circulation in a multimode optomechanical resonator," Nat. Commun. **9**, 1798 (2018).
25. K. Fang, J. Luo, A. Metelmann, M. H. Matheny, F. Marquardt, A. A. Clerk, and O. Painter, "Generalized non-reciprocity in an optomechanical circuit via synthetic magnetism and reservoir engineering," Nat. Phys. **13**, 465–471 (2017).
26. N. R. Bernier, L. D. Tóth, A. Koottandavida, M. A. Ioannou, D. Malz, A. Nunnenkamp, A. K. Feofanov, and T. J. Kippenberg, "Nonreciprocal reconfigurable microwave optomechanical circuit," Nat. Commun. **8**, 604 (2017).
27. G. A. Peterson, F. Lecocq, K. Cicak, R. W. Simmonds, J. Aumentado, and J. D. Teufel, "Demonstration of efficient nonreciprocity in a microwave optomechanical circuit," Phys. Rev. X **7**, 031001 (2017).
28. S. Barzanjeh, M. Wulf, M. Peruzzo, M. Kalaee, P. B. Dieterle, O. Painter, and J. M. Fink, "Mechanical on-chip microwave circulator," Nat. Commun. **8**, 953 (2017).
29. D. Jalas, A. Petrov, M. Eich, W. Freude, S. Fan, Z. Yu, R. Baets, M. Popovic, A. Melloni, J. Joannopoulos, M. Vanwolleghem, C. Doerr, and H. Renner, "What is–and what is not–an optical isolator," Nat. Photonics **7**, 579–582 (2013).
30. H. Xie, C.-G. Liao, X. Shang, M.-Y. Ye, and X.-M. Lin, "Phonon blockade in a quadratically coupled optomechanical system," Phys. Rev. A **96**, 013861 (2017).
31. X.-W. Xu, H.-Q. Shi, A.-X. Chen, and Y.-X. Liu, "Cross-correlation between photons and phonons in quadratically coupled optomechanical systems," Phys. Rev. A **98**, 013821 (2018).
32. Y. Shi, Z. Yu, and S. Fan, "Limitations of nonlinear optical isolators due to dynamic reciprocity," Nat. Photonics **9**, 388–392 (2015).
33. R. Huang, A. Miranowicz, J.-Q. Liao, F. Nori, and H. Jing, "Nonreciprocal photon blockade," Phys. Rev. Lett. **121**, 153601 (2018).
34. G. B. Malykin, "The Sagnac effect: correct and incorrect explanations," Phys. Usp. **43**, 1229–1252 (2000).
35. H. Lü, Y. Jiang, Y.-Z. Wang, and H. Jing, "Optomechanically induced transparency in a spinning resonator," Photon. Res. **5**, 367–371 (2017).
36. H. Jing, H. Lü, S. K. Özdemir, T. Carmon, and F. Nori, "Nanoparticle sensing with a spinning resonator," Optica **5**, 1424–1430 (2018).
37. S. Maayani, R. Dahan, Y. Kligerman, E. Moses, A. Hassan, H. Jing, F. Nori, D. Christodoulides, and T. Carmon, "Flying couplers above spinning resonators generate irreversible refraction," Nature **558**, 569–572 (2018).
38. G. Anetsberger, O. Arcizet, Q. P. Unterreithmeier, R. Rivière, A. Schliesser, E. M. Weig, J. P. Kotthaus, and T. J. Kippenberg, "Near-field cavity optomechanics with nanomechanical oscillators," Nat. Phys. **5**, 909–914 (2009).
39. R. Schilling, H. Schütz, A. H. Ghadimi, V. Sudhir, D. J. Wilson, and T. J. Kippenberg, "Near-field integration of a SiN nanobeam and a SiO_2 microcavity for Heisenberg-limited displacement sensing," Phys. Rev. Appl. **5**, 054019 (2016).
40. C. Doolin, B. D. Hauer, P. H. Kim, A. J. R. MacDonald, H. Ramp, and J. P. Davis, "Nonlinear optomechanics in the stationary regime," Phys. Rev. A **89**, 053838 (2014).

41. G. Brawley, M. Vanner, P. Larsen, S. Schmid, A. Boisen, and W. Bowen, "Non-linear optomechanical measurement of mechanical motion," Nat. Commun. **7**, 10988 (2016).
42. J. Thompson, B. Zwickl, A. Jayich, F. Marquardt, S. Girvin, and J. Harris, "Strong dispersive coupling of a high-finesse cavity to a micromechanical membrane," Nature **452**, 72–75 (2008).
43. H. Jing, D. S. Goldbaum, L. Buchmann, and P. Meystre, "Quantum optomechanics of a Bose-Einstein antiferromagnet," Phys. Rev. Lett. **106**, 223601 (2011).
44. G. Heinrich, J. G. E. Harris, and F. Marquardt, "Photon shuttle: Landau-Zener-Stückelberg dynamics in an optomechanical system," Phys. Rev. A **81**, 011801 (2010).
45. H. Wu, G. Heinrich, and F. Marquardt, "The effect of Landau-Zener dynamics on phonon lasing," New J. Phys. **15**, 123022 (2013).
46. J. T. Hill, "Nonlinear Optics and Wavelength Translation via Cavity-Optomechanics," Ph.D. thesis (California Institute of Technology, 2013).
47. T. K. Paraïso, M. Kalaee, L. Zang, H. Pfeifer, F. Marquardt, and O. Painter, "Position-squared coupling in a tunable photonic crystal optomechanical cavity," Phys. Rev. X **5**, 041024 (2015).
48. H.-K. Li, Y.-C. Liu, X. Yi, C.-L. Zou, X.-X. Ren, and Y.-F. Xiao, "Proposal for a near-field optomechanical system with enhanced linear and quadratic coupling," Phys. Rev. A **85**, 053832 (2012).
49. H. Wang, Q. Qiao, C. Peng, J. Xia, G. Zhou, Y.-J. Zhao, and X.-W. Xu, "Two-dimensional optomechanics formed by the graphene sheet and photonic crystal cavity," arXiv:1806.00798 (2018).
50. C. W. Gardiner and M. J. Collett, "Input and output in damped quantum systems: quantum stochastic differential equations and the master equation," Phys. Rev. A **31**, 3761–3774 (1985).
51. H. J. Carmichael, *An Open Systems Approach to Quantum Optics* (Springer, 1993).
52. G. S. Agarwal and S. Huang, "Electromagnetically induced transparency in mechanical effects of light," Phys. Rev. A **81**, 041803 (2010).
53. S. Weis, R. Rivière, S. Deléglise, E. Gavartin, O. Arcizet, A. Schliesser, and T. J. Kippenberg, "Optomechanically induced transparency," Science **330**, 1520–1523 (2010).
54. A. H. Safavi-Naeini, T. P. M. Alegre, J. Chan, M. Eichenfield, M. Winger, Q. Lin, J. T. Hill, D. E. Chang, and O. Painter, "Electromagnetically induced transparency and slow light with optomechanics," Nature **472**, 69–73 (2011).
55. S. E. Harris, "Electromagnetically induced transparency," Phys. Today **50**, 36–42 (1997).
56. M. Fleischhauer, A. Imamoglu, and J. P. Marangos, "Electromagnetically induced transparency: optics in coherent media," Rev. Mod. Phys. **77**, 633–673 (2005).
57. A. Xuereb, C. Genes, and A. Dantan, "Strong coupling and long-range collective interactions in optomechanical arrays," Phys. Rev. Lett. **109**, 223601 (2012).
58. X.-Y. Lü, Y. Wu, J. R. Johansson, H. Jing, J. Zhang, and F. Nori, "Squeezed optomechanics with phase-matched amplification and dissipation," Phys. Rev. Lett. **114**, 093602 (2015).
59. J.-M. Pirkkalainen, S. Cho, F. Massel, J. Tuorila, T. Heikkila, P. Hakonen, and M. Sillanpaa, "Cavity optomechanics mediated by a quantum two-level system," Nat. Commun. **6**, 6981 (2015).
60. M. J. Burek, J. D. Cohen, S. M. Meenehan, N. El-Sawah, C. Chia, T. Ruelle, S. Meesala, J. Rochman, H. A. Atikian, M. Markham, D. J. Twitchen, M. D. Lukin, O. Painter, and M. Lončar, "Diamond optomechanical crystals," Optica **3**, 1404–1411 (2016).
61. H. Zhang, X. Zhao, Y. Wang, Q. Huang, and J. Xia, "Femtogram scale high frequency nano-optomechanical resonators in water," Opt. Express **25**, 821–830 (2017).
62. J. D. Cohen, S. M. Meenehan, G. S. MacCabe, S. Gröblacher, A. H. Safavi-Naeini, F. Marsili, M. D. Shaw, and O. Painter, "Phonon counting and intensity interferometry of a nanomechanical resonator," Nature **520**, 522–525 (2015).
63. J. Zhang, B. Peng, S. K. Özdemir, Y.-X. Liu, H. Jing, X.-Y. Lü, Y.-L. Liu, L. Yang, and F. Nori, "Giant nonlinearity via breaking parity-time symmetry: a route to low-threshold phonon diodes," Phys. Rev. B **92**, 115407 (2015).
64. I. S. Grudinin, H. Lee, O. Painter, and K. J. Vahala, "Phonon laser action in a tunable two-level system," Phys. Rev. Lett. **104**, 083901 (2010).
65. H. Jing, S. K. Özdemir, X.-Y. Lü, J. Zhang, L. Yang, and F. Nori, "PT-symmetric phonon laser," Phys. Rev. Lett. **113**, 053604 (2014).
66. H. Wang, Z. Wang, J. Zhang, S. K. Özdemir, L. Yang, and Y.-X. Liu, "Phonon amplification in two coupled cavities containing one mechanical resonator," Phys. Rev. A **90**, 053814 (2014).
67. H. Lü, S. K. Özdemir, L.-M. Kuang, F. Nori, and H. Jing, "Exceptional points in random-defect phonon lasers," Phys. Rev. Appl. **8**, 044020 (2017).
68. Y. Jiang, S. Maayani, T. Carmon, F. Nori, and H. Jing, "Nonreciprocal phonon laser," Phys. Rev. Appl. **10**, 064037 (2018).
69. Y.-L. Zhang, C.-L. Zou, C.-S. Yang, H. Jing, C.-H. Dong, G.-C. Guo, and X.-B. Zou, "Phase-controlled phonon laser," New J. Phys. **20**, 093005 (2018).
70. J. Zhang, B. Peng, S. Ozdemir, K. Pichler, D. Krimer, G. Zhao, F. Nori, Y.-X. Liu, S. Rotter, and L. Yang, "A phonon laser operating at an exceptional point," Nat. Photonics **12**, 479–484 (2018).
71. S. Hua, J. Wen, X. Jiang, Q. Hua, L. Jiang, and M. Xiao, "Demonstration of a chip-based optical isolator with parametric amplification," Nat. Commun. **7**, 13657 (2016).
72. K. M. Sliwa, M. Hatridge, A. Narla, S. Shankar, L. Frunzio, R. J. Schoelkopf, and M. H. Devoret, "Reconfigurable Josephson circulator/directional amplifier," Phys. Rev. X **5**, 041020 (2015).